THE JOURNAL OF BIOLOGICAL CHEMISTRY
Vol. 275, No. 51, Issue of December 22, pp. 40425–40433, 2000
© 2000 by The American Society for Biochemistry and Molecular Biology, Inc.
Printed in U.S.A.

New Structural and Functional Aspects of the Type I Interferon-Receptor Interaction Revealed by Comprehensive Mutational Analysis of the Binding Interface*

Received for publication, July 31, 2000, and in revised form, September 12, 2000
Published, JBC Papers in Press, September 12, 2000, DOI 10.1074/jbc.M006854200

Jacob Piehler‡, Laila C. Roisman, and Gideon Schreiber§

From the Department of Biological Chemistry, Weizmann Institute of Science, 76100 Rehovot, Israel

Type I interferons bind to two cell surface receptors, ifnar1 and ifnar2, as the first step in the activation of several signal transduction pathways that elicit an anti-viral state and an anti-proliferative response. Here, we quantitatively mapped the complete binding region of ifnar2 on interferon (IFN)α2 by 35 individual mutations to alanine and isosteric residues. Of the six "hot-spot" residues identified (Leu-30, Arg-33, Arg-144, Ala-145, Met-148, and Arg-149), four are located on the E-helix, which is located at the center of the binding site flanked by residues on the A-helix and the AB-loop. The contribution of residues of the D-helix, which have been previously implicated in binding, proved to be marginal for the interaction with the extracellular domain of ifnar2. Interestingly, the ifnar2 binding site overlaps the largest continuous hydrophobic patch on IFNα2. Thus, hydrophobic interactions seem to play a significant role stabilizing this interaction, with the charged residues contributing toward the rapid association of the complex. Relating the anti-viral and anti-proliferative activity of the various interferon mutants with their affinity toward ifnar2 results in linear function over the whole range of affinities investigated, suggesting that ifnar2 binding is the rate-determining step in cellular activation. Dose-time analysis of the anti-viral response revealed that shortening the incubation time of low-level activation cannot be compensated by higher IFN doses. Considering the strict dependence of the cellular response on affinity, these results suggest that for maintaining transcription of IFN-responsive genes over a longer time period, low but continuous signaling through the IFN receptor is essential.

Type I interferons (IFN)[1] are a family of homologous cytokines, which potently elicit an anti-viral and anti-proliferative state in cells. All human type I IFNs (IFNα, β, ω, and τ) bind to a cell surface receptor consisting of two transmembrane proteins, ifnar1 (1) and ifnar2 (2), which associate upon binding. Binding of IFN to its receptor mediates activation of numerous genes (3) through different signal transduction pathways (reviewed in Ref. 4). Intriguingly, different expression profiles are induced by different IFNs, apparently through the same receptor, with particular differences between IFNα and IFNβ (3, 5). However, the molecular mechanisms underlying the functional differences between IFNs are still unknown. Type I IFNs belong to the class of helical cytokines (6) and are built by five helices. The structure of several type I IFNs have been resolved, such as murine IFNβ (7), human IFNα2 (8, 9), human IFNβ (10), and ovine IFNτ (11). Mutational studies have revealed functionally important residues on IFNs (reviewed in Ref. 12), which can be ascribed to distinct functional epitopes that interact with ifnar1 and ifnar2 (13, 14). The binding site for ifnar2 was mainly mapped on the AB-loop and D-helix and the binding site for ifnar1 on the C-helix. However, comparison with homologous cytokines suggests the involvement of the E-helix in the binding of ifnar2 (8, 13, 15).

Understanding the basis of IFN signaling at the molecular level requires establishing in quantitative terms the correlation between IFN cellular activity and its structural, kinetic, and thermodynamic binding parameters for its receptors. Having established methods for expression, refolding, and purification of the extracellular domain of ifnar2 (ifnar2-EC), we have recently analyzed the kinetics and thermodynamics of the interaction between ifnar2-EC and IFNα2 by solid phase detection (16). We mapped the binding interface of IFNα2·ifnar2-EC by single alanine mutations and determined the precise energetic contribution of individual residues in the complex (16, 17). Only very minor contributions of residues on the D-helix were observed, and only three residues on the AB-loop contributed more than 1.0 kcal/mol, suggesting additional elements of IFNα2 are involved in binding ifnar2. In this study, we present a complete high-resolution map of the binding site of IFNα2 for ifnar2 in energetic and kinetic terms. Based on a large set of single-residue IFNα2-mutants covering several orders of magnitude in binding affinity, we have correlated the cellular activity exerted by these IFNs with the structural, thermodynamic, and kinetic parameters of their interaction with ifnar2-EC.

EXPERIMENTAL PROCEDURES

Materials—EDC and NHS were purchased from Fluka. Monoclonal anti-ifnar2-EC 46.10 and 117.7, which bind non-competitively and do not inhibit IFN binding, were a gift from Daniela Novick, (Weizmann Institute of Science). WISH and Daudi cells were a gift from Daniela Novick.

Protein Expression and Purification—IFNα2 and ifnar2-EC were expressed in *Escherichia coli* and purified by ion exchange and size-exclusion chromatography as described earlier (16, 17). Protein concentrations were determined from the absorbance at 280 nm (16) with ϵ_{280} = 18,070 M^{-1} for IFNα2 and ϵ_{280} = 26,500 M^{-1} for ifnar2-EC. Protein

* This work was supported by Grant 96-00439/1 from the United States-Israel Binational Science Foundation (BSF). The costs of publication of this article were defrayed in part by the payment of page charges. This article must therefore be hereby marked "*advertisement*" in accordance with 18 U.S.C. Section 1734 solely to indicate this fact.

‡ An EMBO Postdoctoral Fellow, 1998-1999.

§ Incumbent of the Dewey David Stone and Harry Levine Career Development Chair. To whom correspondence should be addressed. Tel.: 972 8 934 3249; Fax: 972 8 934 4118; E-mail: bcges@weizmann.ac.il.

[1] The abbreviations used are: IFN, interferon; ifnar, type I interferon receptor; mAb, monoclonal antibody; EC, extracellular domain; EDC, ethyl-dimethylaminopropyl carbodiimide; NHS, N-hydroxysuccinimide; RIfS, reflectometric interference spectroscopy; BIA, biomolecular interaction analysis; VSV, vesicular stomatitis virus; wt, wild-type; STAT, signal transducers and activators of transcription.

purity was analyzed by SDS-polyacrylamide gel electrophoresis under non-reducing conditions, and concentrations were verified by quantitative evaluation of the protein bands compared with wild-type standard. The concentration of active IFNα2 protein was determined for all mutants by analytical gel filtration with ifnar2-EC as described earlier (16).

Site-directed Mutagenesis—Site-directed mutagenesis was carried out by polymerase chain reaction amplification of the complete plasmids for expression (pT72Cα2) with 18–21 nucleotide primers containing the mutated codon using high fidelity polymerases *pwo* (Roche Molecular Biochemicals) and *pfu* (Stratagene) as previously described in detail (18). After phosphorylation and ligation, the mutated plasmids were transformed into *E. coli* TG1 cells. The sequence of the whole expressed gene containing the mutation was verified by DNA sequencing.

Measurements of Kinetics and Affinity—The interaction between recombinant ifnar2-EC and IFNα2 was monitored by an optical probe called reflectometric interference spectroscopy (RIfS) under flow-through conditions (19). This method detects biomolecular interaction at interfaces as a change in the apparent optical thickness of a thin silica layer. The complete experimental setup for this methodology has been previously described in detail (20, 21). Binding to the surface is monitored as a shift in the interference spectrum. A shift of 1 pm corresponds to approximately 1 pg/mm^2 protein on the surface. All measurements were carried out using HBS (20 mM HEPES, pH 7.5, 150 mM NaCl, and 0.01% Triton X-100) as a running buffer. The non-neutralizing anti-ifnar2-EC mAb 46.10 was covalently coupled to the carboxyl-functionalized dextran layer on the transducer surface by standard BIAcore protocols. Ifnar2-EC (20 μg/ml, 800 nM) was captured by the immobilized antibody, followed by cross-linking with a second mAb (117.7) at a concentration of 10 μg/ml (65 nM). The binding curves were evaluated with the BIAevaluation software (Biacore AB, Sweden) using simple one-to-one kinetics models. For the determination of dissociation constants K_D, the equilibrium response was plotted *versus* the concentration and fitted by the law of mass action.

Anti-viral Protection Activity Assay—Anti-viral activity of wild-type and mutant IFNα2 was assayed as the inhibition of the cytopathic effect of vesicular stomatitis virus (VSV) on human WISH cells (22). The relative activity of IFNα2-mutants was determined as the concentration needed for 50% protection of the cells relative to the concentration of wild-type IFNα2 needed for 50% protection. Dose-time experiments were carried out by occluding free interferon after different incubation times. At time 0, IFNα2 was added at concentrations between 1 and 250 pM to a culture of human WISH cells. At different time points, a quantity of ifnar2-EC was added (1–5 μM), which was calculated to reduce the free IFN concentration in the sample to less than 0.5 pM, which was below the threshold for cell protection in our assay. In all cases, the culture was challenged with VSV 4 h after the addition of IFNα2. After 18 h of growth, the cells were stained with crystal violet to determine the proportion of intact cells.

Anti-proliferative Assay—The anti-proliferative activity of IFNα2 on Daudi cells was assayed as follows. Two-fold serial dilutions of IFNα2 (10–12 samples altogether) were prepared in flat-bottomed 96-well plates, with final concentrations of wild-type IFNα2 ranging from 0.04 to 82 pM. The concentration range for IFNα2 mutants was adjusted according to the anticipated anti-proliferative activity for the specific mutant as estimated from its affinity. 100 μl of human Daudi Burkitt's lymphoma cells growing in RPMI 1620 supplemented with 10% fetal calf serum and 4 mM L-glutamine were added into each well and were grown for an additional 60 h with IFN. The number of living cells was then determined using a cell staining kit (Biological Industries Co, Israel) based on the colorimetric detection of the cleavage of the tetrazolium salt XTT into formazan. The XTT reaction solution was added according to the manufacturer's recommendation for a period of 5 h, after which the absorbance at 475 nm was recorded in an ELISA-reader. The relative anti-proliferative activities of IFNα2-mutants were determined as the concentration needed for 50% inhibition of cell growth relative to the concentration of wild-type IFN needed for 50% inhibition.

RESULTS

Binding Assays by Label-free Detection—The interaction of IFNα2 with ifnar2-EC was characterized by a biosensor system based on reflectometric interference spectroscopy (RIfS) using purified proteins for all measurements. In previously published experiments, ifnar2-EC was covalently immobilized via its exposed amino groups by amine-coupling chemistry (17). From these studies, a dissociation constant of about 10 nM was determined for the wild-type IFNα2·ifnar2-EC complex, with an association rate constant of 2×10^6 M^{-1} s^{-1} and a dissociation rate constant of 0.02 s^{-1}. Because we observed heterogeneous affinity of covalently coupled ifnar2-EC, we investigated alternative methods for immobilization including biotinylated ifnar2-EC and capturing with monoclonal antibodies (mAb). An efficient protocol was developed based on affinity capturing and cross-linking with two different monoclonal anti-ifnar2-EC antibodies (46.10 and 117.7) that bind ifnar2-EC non-competitively and do not interfere with interferon binding; ifnar2-EC was captured from the solution by the surface bound mAb 46.10, followed by cross-linking with mAb 117.1, which virtually abolished leak-out because of dissociation. This method of immobilization provided a stable surface, which was readily regenerated by a short pulse of 50 mM HCl. Thus, the immobilized mAb 46.10 could be repeatedly reloaded with fresh ifnar2-EC. In addition to the simple regeneration of this surface, we observed a significant improvement in the homogeneity of the ifnar2-EC binding sites compared with measurements done using the standard amine coupling method. This proved to be particularly advantageous for retrieving direct binding data for some of the weaker binding IFNα2 mutants (*e.g.* R33A), which could not be measured using the standard amine-coupling method. A comparison of IFNα2 binding to ifnar2-EC immobilized to the surface via both methods clearly shows that absolute rates of association and dissociation differ (Fig. 1*a*), with the affinity of IFNα2 toward mAb-immobilized ifnar2-EC being 2.5-fold higher than toward the amine-coupled receptor. The difference in affinity is a result of a faster k_a and a slower k_d (Fig. 1*a*). However, the relative changes of rate constants and affinities upon mutation of IFNα2 were in good agreement, as demonstrated in Fig. 1*b*. Thus, the changes in free energy of interaction upon mutation ($\Delta\Delta G^0$) determined from measurements on both surfaces were consistent.

The time resolution in solid phase detection is typically limited to the subsecond range because of the inertia of flow-through sample handling. With the biosensor system used in this study, dissociation rate constants of up to ~0.3 s^{-1} were properly resolved, which is about 30-fold faster than the rate measured for the interaction of the wild-type proteins. The dissociation of several low-affinity IFNα2 mutants was too fast to be directly determined. In these cases, the affinity was determined from the concentration dependence of the equilibrium binding response on the sensor surface. The binding affinities as calculated from the rate constants corresponded well to those obtained from analysis of the equilibrium response (Fig. 1*c*).

Mapping the Binding Site of IFNα2 for ifnar2—The AB-loop and to a lesser extent the D-helix have been previously identified as being important for IFN activity and ifnar2 binding (12). However, mapping these residues on the structure of IFNα2 (17), as well as homology considerations, raised the possibility that the binding interface extends toward the E-helix. Here, most surface exposed residues of the E-helix were individually mutated to Ala, and their contribution to binding was determined. The mutations R144A, A145G, M148A, and R149A each resulted in a decrease in binding affinity of over 20-fold, corresponding to a loss of more than 2 kcal/mol of binding free energy (Table I and see Fig. 4*a*) (the D146A mutant did not refold and thus could not be measured). The mutations S152A and L153A reduced binding by 6- and 13-fold, respectively, whereas mutation N156A had no significant effect on binding (Table I). Extending the search to the A-helix revealed that Leu-15 was also involved in the interaction with ifnar2, whereas mutating Met-16 had no effect on binding. On the

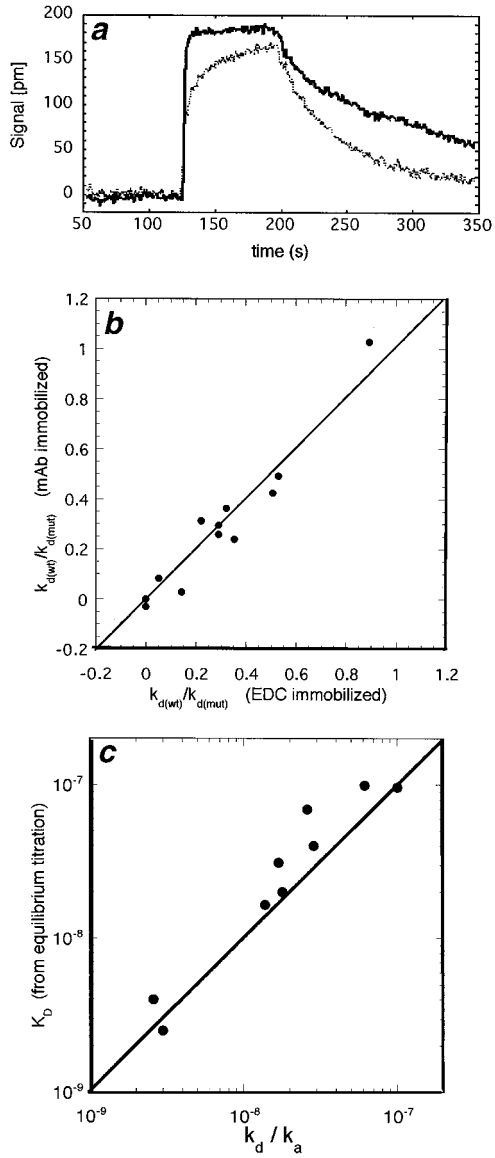

FIG. 1. **Binding of IFNα2 to ifnar2-EC measured by heterogeneous phase detection in real time by RIfS.** *a*, binding of IFNα2 (500 nM) to ifnar2-EC immobilized to the surface by affinity capturing and cross-linking compared with the same binding experiment with ifnar2-EC coupled with EDC/NHS. *b*, relative change in k_d of mutants of IFNα2 in complex with ifnar2-EC bound to the surface by EDC/NHS cross-linking *versus* affinity capturing. Data for ifnar2-EC cross-linked via EDC/NHS are from Ref. 17. Data for affinity capturing are from this work. Only values of k_d of mutants that have been determined by both methods are included. *c*, binding affinities (K_D) of mutants of IFNα2 in complex wild-type ifnar2-EC, as determined from different equilibrium surface loadings *versus* values of K_D determined from the ratio of k_d/k_a. Data are from Table I.

D-helix, only Lys-133 contributed more than 0.5 kcal/mol of binding free energy. Although most of the residues on the AB-loop have been analyzed previously (17), these results were confirmed here with ifnar2-EC immobilized via mAbs. Furthermore, the K_D of mutants with extremely low affinity were quantified appropriately. On the AB-loop, residues Leu-30 and Arg-33 contributed 3.8 and 5.5 kcal/mol binding free energy (relative to Ala). Leu-26, Phe-27, Lys-31, Asp-32, and His-34 contributed between 0.5–2 kcal/mol of binding free energy (Table I), whereas residues Arg-22, Arg-23, Ile-24, Ser-25, Ser-28, Asp-35, and Gln-40 do not contribute significantly to binding. For most of the mutations, the change in binding affinity was dictated by a change in k_d, whereas k_a was constant. The exceptions were R144A, where k_a decreased 10-fold whereas k_d increased by 4-fold, and K133A where k_a decreased by 5-fold whereas k_d increased by less then 2-fold. Thus, in these cases the mutations affected mostly k_a (Table I).

Mapping the change in binding free energy upon mutation on the structure of IFNα2 gives a consistent picture of the binding site (Fig. 2*a*). Six hot-spot residues are located in the center of the binding site, each of them decreasing $\Delta\Delta G^0_{\text{mut-wt}}$ by more than 2 kcal/mol (Leu-30, Arg-33, Arg-144, Ala-145, Met-148, and Arg-149, *red*). Nine additional residues contribute between 0.5–2 kcal/mol (Leu-15, Leu-26, Phe-27, Lys-31, Asp-32, His-34, Lys-133, Ser-152, and Leu-153). Residues that contribute less then 0.5 kcal/mol of free binding energy, and thus are probably not within the binding interface, surround the residues mapped within the binding site. The binding site is composed of residues in the A- and E-helices and the AB-loop, with the hot-spot residues being located at the center of the binding site (Fig. 2*b*).

In the published NMR structure of IFNα2, the C-terminal is not involved in any specific interaction with the rest of the protein and seems to be flexible. To assess the importance of the C-terminal residues to IFN activity, a truncated IFNα2 protein (missing the five last residues) was produced. Analytical gel filtration in the absence and presence of ifnar2-EC demonstrated that this protein folds correctly and retains ifnar2 binding activity (data not shown). Similar affinity and rate constants were found for the truncated protein compared with the wild-type protein (Table I). Thus, the C terminus of IFNα2 does not seem to participate in ifnar2 binding. Previous studies of C-terminal-truncated interferons have given mixed results, from retaining most of the antiviral activity (23) to losing most of it (for fragment 1–158, Ref. 24).

Isosteric Mutations of Leu-30 and Arg-33—A significant advantage of immobilizing ifnar2-EC by affinity capturing is the low level of nonspecific background, even at very high IFNα2 concentrations. Consequently, we could directly determine the binding affinities of the IFNα2 mutations L30A, L30V, R33A, R33K, and R33Q, a task not feasible with ifnar2-EC immobilized by amine-coupling. An Ala at position 30 reduced the binding affinity toward ifnar2-EC to 1.7 μM, whereas the R33A mutant had an affinity of 28 μM. The cause for the large decrease in affinity of these two mutations was further investigated by isosteric mutations. The binding affinity of L30V is 260 nM (compared with 4 nM of the wild-type), thus most of the binding is lost by shortening the branched side chain by a single methylene unit. For Arg-33, the regain of binding affinity upon introducing isosteric mutations was even smaller; an affinity of 8 μM was determined for R33K, whereas R33Q caused a decrease in affinity to 86 μM. The small difference in binding affinity between R33A and R33K is surprising, as Lys was often found to replace Arg without much change in binding or activity. Possibly, mutating Arg-33 affects the structural integrity of the binding site.

Anti-viral Activity Versus Affinity of IFNα2 Mutants—Binding of IFN to ifnar2 is the very first step initiating a complex signal transduction cascade that activates the anti-viral state in cells. The interferon concentration which gives 50% protection of human WISH cells challenged with VSV is a good measure for its biological activity. Here, the concentrations giving rise to 50% protection (I_{50}^{mut}) for the various IFNα2 mutants were determined. The relative anti-viral activity p_{AV} was obtained by normalizing to the concentration measured for wild-type IFNα2 (I_{50}^{wt}) with $p_{AV} = I_{50}^{wt} / I_{50}^{mut}$. Previously, a good correlation between the binding affinity and the anti-viral activity was observed for a set of mutants located in the AB-loop and the D-helix (17). Here, this correlation is extended to vir-

TABLE I
Thermodynamic and kinetic constants for the interactions of mutant IFNα2 with wild-type ifnar2-EC

IFNα2 mutant	k_a[a] 10^6 M^{-1} s^{-1}	k_d[a] s^{-1}	K_D[b] nM	K_D[c] nM	$\Delta\Delta G^0_{mut\text{-}wt}$[d] kcal/mol	$\Delta\Delta G^0_{mut\text{-}wt}$[e] kcal/mol
α2 wt	3.7	0.011	3.0	2.5		
L15A	2.8	0.073	26.0	69	1.3	2.0
M16A	3.7	0.014	3.7		0.1	
R22A	3.7	0.015	4.0		0.2	
R23A	3.2	0.018	5.5		0.4	
I24A	4.6	0.011	2.4		−0.1	
S25A	3.2	0.008	2.6	4	−0.1	0.3
L26A	3.0	0.050	16.9	31	1.0	1.5
F27A	2.0	0.027	13.7		0.9	
L30A				1700		3.8
L30V				259		2.7
K31A	2.2	0.020	9.0		0.7	
D32A	3.0	0.026	8.7		0.6	
R33K				8000		4.8
R33A				28100		5.5
R33Q				86200		6.2
H34A	2.4	0.019	7.9		0.6	
D35A	4.0	0.018	4.6		0.3	
Q40A	3.9	0.012	3.1		0.0	
R125A	5.1	0.016	3.0		0.0	
K131A	2.0	0.012	6.2		0.4	
E132A	5.2	0.011	2.1		−0.2	
K133A	0.7	0.018	26.0		1.3	
K134A	3.6	0.014	3.8		0.1	
R144A	0.36	0.043	120	99	2.2	2.2
A145G	2.9	0.288	100.0	96	2.1	2.2
A145M	4.4	0.079	17.9	20	1.1	1.2
M148A				143		2.4
R149A				538		3.2
S152A	3.6	0.049	13.8	16.5	0.9	1.1
L153A	3.7	0.105	28.6	40	1.3	1.6
N156A	3.7	0.010	2.6		−0.1	
L161Z	3.2	0.015	4.5		0.2	

[a] All rate constants were measured by heterogeneous phase detection with ifnar2-EC affinity captured on the surface. The standard deviations from at least three independent measurements were $\sigma = 10\%$ for all k_d and $\sigma = 15\%$ for all k_a.
[b] Determined from the rate constants $K_D = k_d/k_a$, $\sigma < 20\%$.
[c] $K_{D(eq)}$ is determined from equilibrium binding at the surface. The standard error is ~25%.
[d] $\Delta\Delta G^0 = \Delta G^0_{mut} - \Delta G^0_{wt}$, with ΔG^0 calculated from $\Delta G^0 = RT\ln k_d/k_a$. ΔG^0_{wt} equals 11.6 kcal/mol, and $\sigma = 0.16$ kcal/mol.
[e] $\Delta\Delta G^0_{eq} = \Delta G^0_{eq(mut)} - \Delta G^0_{eq(wt)}$, with ΔG^0 calculated from $\Delta G^0 = RT\ln K_D$, with K_D determined from equilibrium binding to the surface (see Footnote c). ΔG^0_{wt} equals 11.7 kcal/mol, $\sigma = 0.2$ kcal/mol.

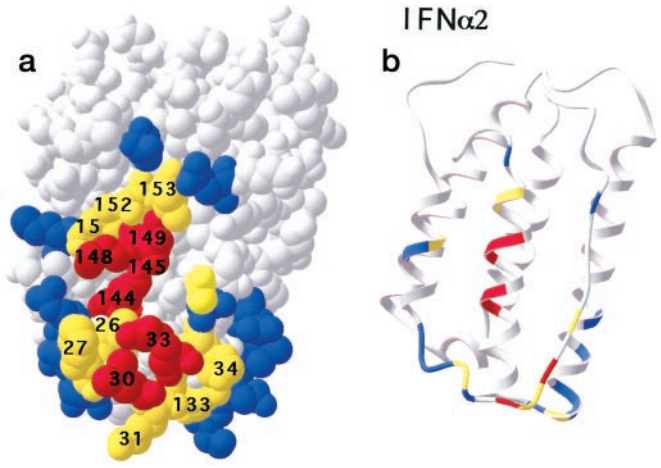

FIG. 2. **The functional epitope for binding ifnar2 on IFNα2 (solution structure of IFNα2-(1–161) according to Ref. 8).** *a, space-filling* representation; *b, ribbon* model. Hot-spot residues ($\Delta\Delta G^0 > 2$ kcal/mol) are colored *red*, other residues with significant effect on complex stability ($\Delta\Delta G^0$ of 0.5–2.0 kcal/mol) are colored *yellow*. Indifferent residues are depicted in *blue*. This picture was composed with the Swiss-PDB Viewer (36).

tually a complete set of residues involved in the interaction of IFNα2 with ifnar2-EC, covering 4 orders of magnitude of binding affinities. To weigh binding affinities over this whole range equally, we correlated this data on a logarithmic scale. An excellent linear correlation between the affinity of IFNα2 toward ifnar2-EC and anti-viral activity was observed for all mutants (Fig. 3*a*). The slope of this curve is 0.72, which is probably because of the constant contribution of ifnar1 toward formation of the active ternary complex. Notably, the relation between affinity and activity is maintained also for R144A and K133A. In these two cases, the affinity is mainly affected by a large reduction in k_a (10- and 5-fold, respectively). Thus, anti-viral activity is related to the binding affinity, independent of the relative contributions of k_a and k_d. Truncating IFNα2 at residue Ser-160 had no significant effect on the anti-viral activity compared with the wild-type protein, thus confirming that the five C-terminal residues are not essential for IFN function.

Anti-proliferative Activity Versus Affinity of IFNα2 Mutants—The level of the anti-proliferative response of IFN on Daudi cells is a well established marker that determines the potency of IFNs. Furthermore, it has been suggested that the anti-proliferative response is mediated by different elements of the signal transduction pathways than those mediating anti-viral activity (4). Anti-proliferative activity of the various IFNα2 mutants was determined by measuring the relative number of living cells 60 h after the addition of IFNα2, using a colorimetric assay (detecting the cleavage of the tetrazolium salt XTT to formazan). For exponentially growing Daudi cells, ~0.3 pM wild-type IFNα2 incubated over 60 h was required to inhibit cell growth by 50% (Fig. 3*b*). Plotting the relative anti-proliferative potency of the various IFNα2 mutants *versus* their

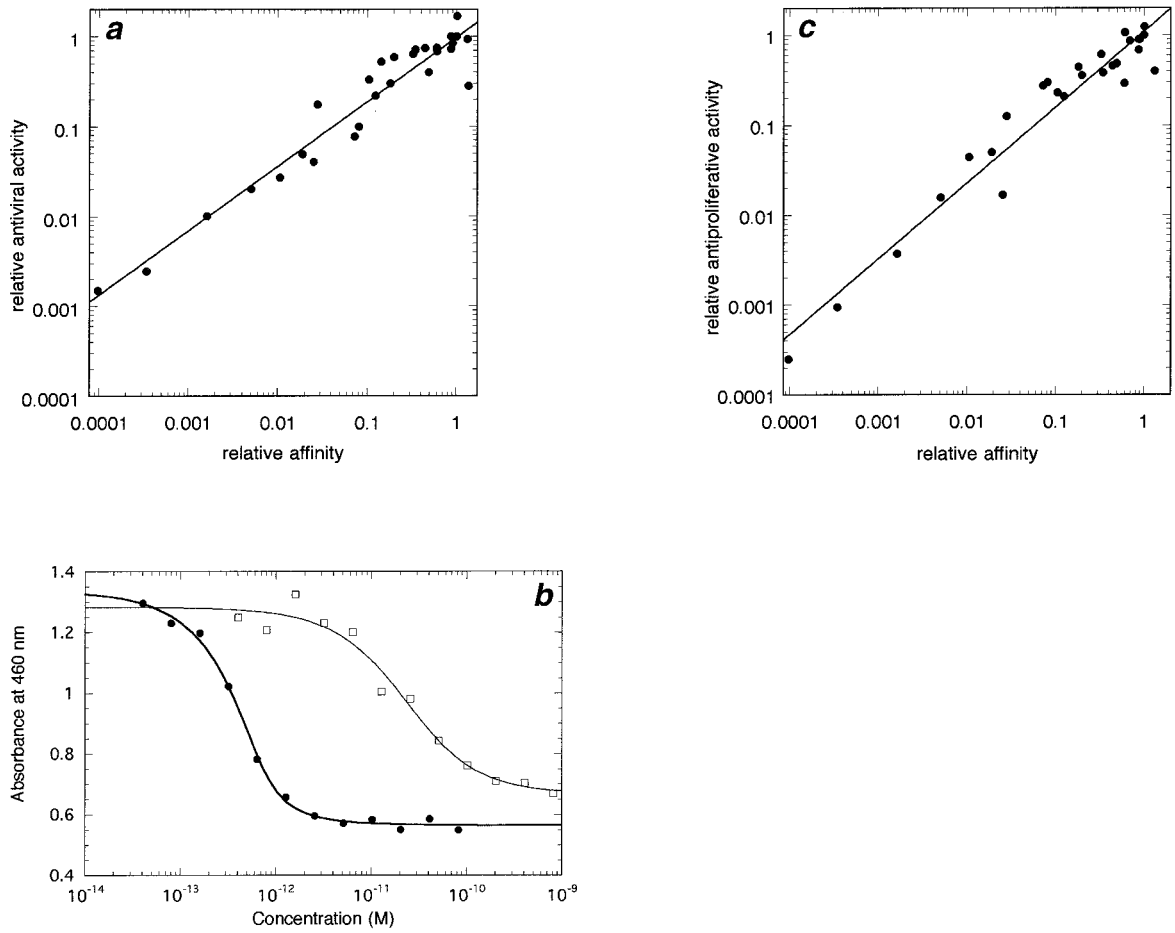

FIG. 3. **Biological activity of IFNα2 mutants.** *a,* correlation between affinity and the relative anti-viral response of different IFNα2 mutants (correlation coefficient of 0.965). *b,* representative dose-response curves from the anti-proliferative assay for IFNα2 wild-type (*filled circles*) and R149A (*open squares*). *c,* correlation between affinity and the relative anti-proliferative activities (correlation coefficient of 0.97).

relative binding affinity toward ifnar2-EC yielded a linear correlation (Fig. 3*c*). The slope of the (logarithmic) affinity-activity plot is 0.84.

A detailed graphic comparison of the relative contributions toward binding and activity of the individual residues is presented in Fig. 4. On the AB-loop, only two residues (Leu-30 and Arg-33) caused a significant decrease in all three parameters. Except for Lys-133, none of the residues located on the D-helix are involved in binding or in biological activity. Many of the residues on the E-helix are important for binding and activation of the biological response. Within the error of the assays, the relative contribution to binding are in agreement with the changes in biological activity.

Time-dose Relationship for Activating the Anti-viral Response—IFN-induced association of ifnar1 and ifnar2 causes phosphorylation and activation of STAT. It has previously been observed that the initiation of the anti-viral state depends on the continuous presence of interferon for at least 4 h prior to viral infection (25). Here we wanted to determine whether higher concentrations of interferon (which increases the number of activated receptors) would shorten the time needed to activate the anti-viral state. The availability of large amounts of purified ifnar2-EC enabled us to elegantly block receptor stimulation by IFN after specific time periods. Complete protection was achieved at an IFNα2 concentration of 16 pM after at least a 4-h incubation in the presence of IFNα2, prior to its occlusion by ifnar2-EC (Fig. 5). Occluding free IFNα2 from the medium after less than 4 h did not result in the activation of the anti-viral state. Adding interferon at much higher concentrations (up to 250 pM) did not shorten the time of continuous interferon presence needed to activate the anti-viral state (Fig. 5). This is despite the larger number of activated receptor complexes per cell expected at higher IFNα2 concentrations.

DISCUSSION

Structural and functional aspects of IFN signaling through its receptors ifnar1 and ifnar2 are currently understood only on a basic level. IFN-induced association of the receptors stimulates a variety of signaling transduction pathways by activating the associated kinases Jak1 and Tyk2. However, the fact that different IFNs elicit different response profiles through the same receptor requires detailed correlation of structural and functional properties of IFNs. Here we present a virtually complete high-resolution picture of the ifnar2-binding epitope of IFNα2, obtained by extensive mutational analysis using direct binding assays to evaluate affinity and kinetics of the interaction between IFNα2 and ifnar2-EC. Based on a large set of IFNα2 mutants, we investigated in detail the role of kinetics and affinity of the IFNα2-ifnar2 interaction for IFN signaling and activity. By individually mutating many of the surface-exposed residues located on helices A, D, and E, as well as on the AB-loop to Ala, we quantitatively mapped their energetic contributions. We located the ifnar2 binding site on the first half of the AB-loop (residues 26–34), residue 133 on the D-helix, the E-helix (residues 144–153), and on a small part of the A-helix (L15). Two additional residues that may affect binding are Arg-12 and Glu-146, but the corresponding Ala mutants failed either to express or fold. Mutating Glu-146 to Lys was

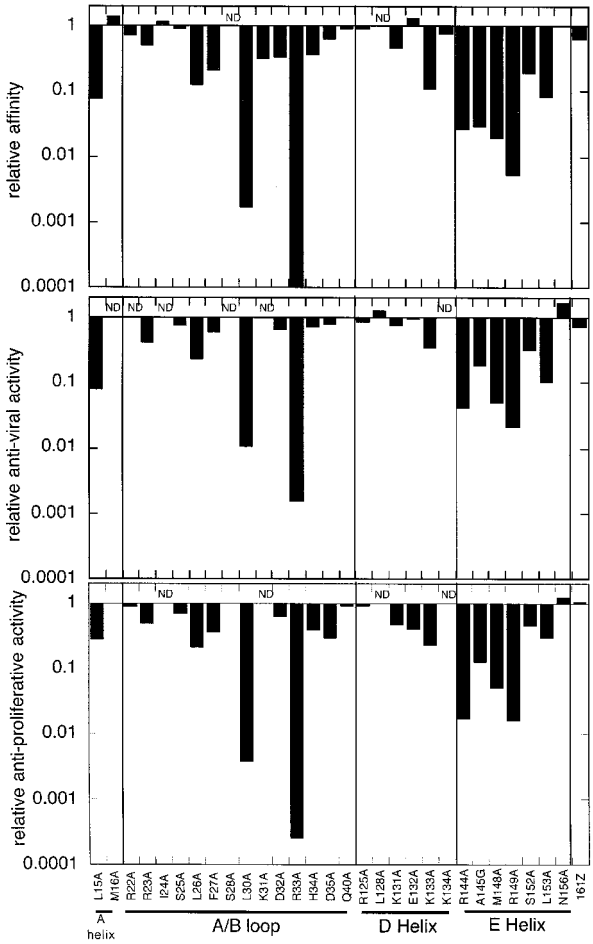

FIG. 4. **Relative binding affinity toward ifnar2-EC measured in RIfS, anti-viral response, and anti-proliferative response of all Ala mutants of IFNα2 analyzed in this work**.

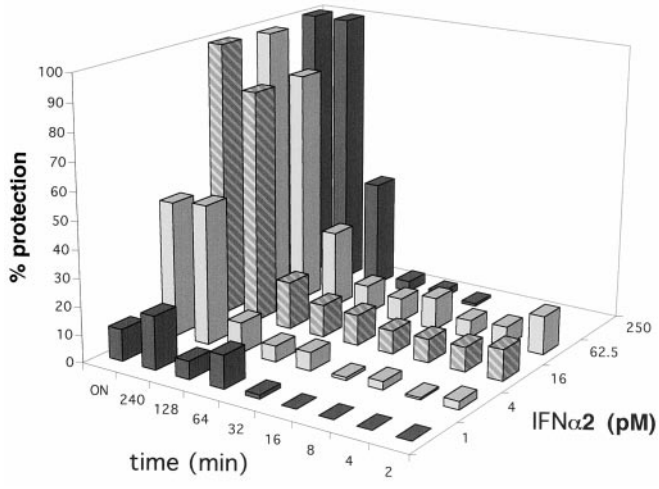

FIG. 5. **Kinetics of formation of the anti-viral state at a range of IFNα2 concentrations.** IFNα2 was added at time 0 to a growing culture of WISH cells. Ifnar2-EC (1–5 μM final, depending of the concentration of IFNα2) was added at different time points to occlude any free IFNα2 from the solution. The *lane* marked *ON* is a control where no ifnar2-EC was added. Four hours after adding IFNα2, the culture was challenged with VSV. The next day, the culture was stained with crystal violet to determine the proportion of living cells from which the percent protection was calculated.

previously shown to cause a large reduction in biological activity, albeit this was explained as resulting from the role of Glu-146 in stabilizing the AB-loop (26). In the center of the ifnar2 binding site is the E-helix, flanked by helix A and the AB-loop from both sides. The D-helix faces a different surface of the protein than the suggested binding site, in agreement with its marginal contribution to binding of ifnar2 (Fig. 2*b*). Coloring all mutated residues according to their contribution to binding (Fig. 2*a*) shows that the ifnar2 binding site on IFNα2 is surrounded by inert residues (*blue*). Assuming that the interface consists of a continuous surface patch, we conclude that most of the ifnar2 binding site has been identified. The classical interface structure consists of hot-spot residues ($\Delta\Delta G^0 > 2$ kcal/mol) located at the center of the binding site, surrounded by residues, which have a smaller impact on binding (27, 28). On IFNα2, Ala-145 is located at the center of a pocked, enclosed by Arg-22, Leu-26, Phe-27, Arg-33, Arg-144, Met-148, and Met-149 (Fig. 2*a*). All of these residues, except for Arg-22, were found to contribute significantly to binding, including 5 of the 6 hot-spot residues identified (except for Leu-30). Residues Leu-15, Ala-19, Ile-24, Ser-28, Leu-30, Lys-31, His-34, Asp-35, Lys-133, Ser-152, and Leu-153 form the next shell surrounding this core of the binding site. From this group of residues, only Leu-30 contributes more than 2 kcal/mol to binding, whereas Leu-15, Lys-31, His-34, Ser-152, and Leu-153 contribute between 0.5–2 kcal/mol of free energy of binding. Removing the five terminal residues of IFNα2 (161–165) did not affect binding to ifnar2-EC, nor did it have any effect on the magnitude of biological anti-viral or anti-proliferative activity. As these residues are conserved in most human interferons (but are truncated in IFNα7), their biological role in a whole organism needs further evaluation.

About half of the 18 residues surrounding Ala-145 are hydrophobic. The hydrophobicity of the ifnar2 binding site relative to the IFNα2 protein surface was calculated using the computer program QUILT, which calculates hydrophobic patches on protein surfaces (29). The largest continuous hydrophobic patch on IFNα2 overlays with the ifnar2 binding site, as determined by mutagenesis (Fig. 6). Strikingly, performing this calculation on a model of ifnar2 identified the IFNα2 binding site on ifnar2 also as the largest continuous hydrophobic patch on ifnar2 (Fig. 6). Although the IFNα2-ifnar2 binding interface is hydrophobic, electrostatic forces have been shown to play a significant role in steering these two proteins to achieve fast binding (16). The electrostatic potential on IFNα2 at the ifnar2 binding site is clearly positive (Fig. 6). This positive potential stems from the many Arg and Lys residues located both within and around the binding site (9 *versus* only 5 Asp+Glu). Interestingly, performing a similar analysis on the IFNα2 binding site on ifnar2 shows that, although this binding site exerts a strong negative electrostatic potential, most of the negatively charged residues seem to be located either at the periphery or outside the physically interacting surfaces (Fig. 6 and Ref. 17). From the large complementary hydrophobic binding surfaces between IFNα2 and ifnar2, it is speculated that hydrophobic interactions are of major importance in stabilizing this complex, whereas charged residues, many of which are located at the periphery of the binding site, are important in steering these two proteins together (30, 31).

The sequence homology between different IFNαs is ~70% and 30% between IFNα and IFNβ. Comparison of functionally important residues on a sequence alignment of different type I IFNs shows that some of the residues interacting with ifnar2 are not fully conserved, including some of the hot-spot residues on the A- and E-helices (Fig. 7); Leu-15 is a Met in IFNα5 and a Cys in IFNβ. Ala-145 is a Met in IFNω and a Val in IFNβ. The dissociation constant K_D of the A145M mutation (in IFNα2) is 5-fold lower than A145G, yet 8-fold higher than Ala at this position (see Table I). Met-148 is a Leu in IFNβ, Ser152 is a Tyr

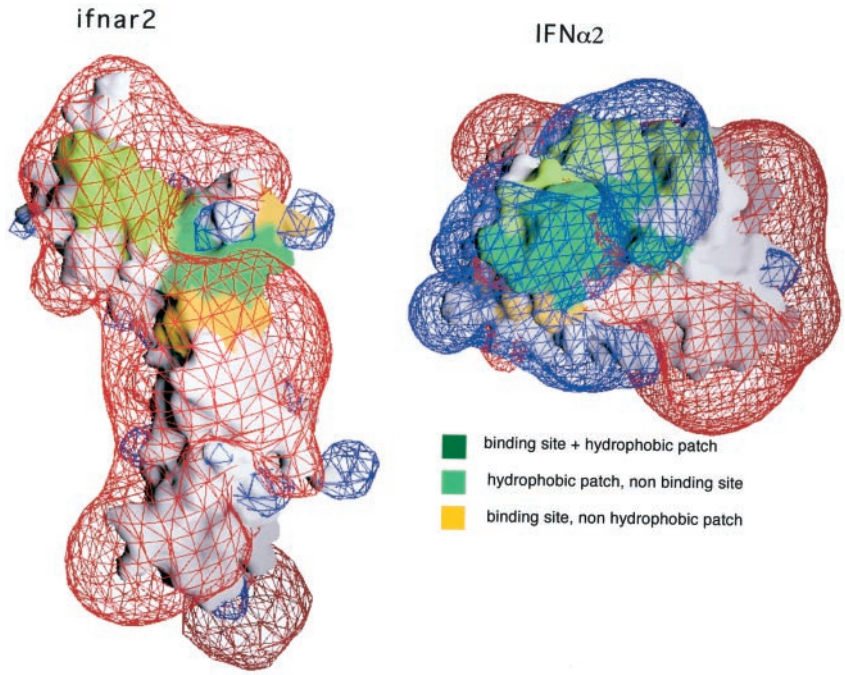

FIG. 6. **Hydrophobic and electrostatic surface representation of IFNα2 and ifnar2-EC.** The largest continuos hydrophobic patch on the protein surfaces, as identified using the computer program QUILT (29) is colored *green*. *Dark green*, hydrophobic patch overlapping the binding site; *light green*, hydrophobic patch does not overlap the binding site; *yellow*, binding site does not overlap the hydrophobic patch. The binding site was determined through mutagenesis. The electrostatic potential was calculated using the computer program GRASP (36), with the ionic strength set at 0.1 M. The contours are drawn at 0.7 kT/e (*blue,* positive potential; *red,* negative potential). The structure of IFNα2 is from Ref. 8, and the structure of ifnar2-EC is modeled according to its homology to ifnaγR (17, 37).

and Leu-153 is a Val. Interestingly, Leu-153 is not fully conserved between different IFNαs either. Comparing the binding epitopes for IFNα2 and IFNβ on ifnar2 indicates that both proteins interact with a similar set of residues, but with a very different relative contribution of binding energies within the binding site (17, 32). This observation can be rationalized from the partial conservation of active site residues on IFNα2 and IFNβ. Two of the six hot-spot residues and six of the nine remaining residues that contribute to binding are not conserved between these two interferons. In contrast to IFNβ, all six hot-spot residues on IFNα2, and eight of the nine remaining active-site residues were found to be conserved on 10 of the 11 IFNαs aligned.

A structure-function analysis of the ifnar2 binding site on IFNβ has identified the A- and E-helices as well as the AB-loop as constituting the ifnar2 binding site (33). A quantitative comparison between the results presented here and those of Runkel *et al.* (33) is difficult. First, there are differences in the methods of measurements, second, whereas we analyzed single mutations, Runkel *et al.* (33) analyzed multiple mutations only. However, some qualitative differences between IFNα2 and IFNβ seem to emerge. Whereas in IFNβ residues Lys-135 and Glu-136 (homologous to Lys-133 and Lys-134 in IFNα2) increase receptor binding affinity, they decrease anti-proliferative activity by 10-fold. In IFNα2, the mutation K134A had no effect on binding, whereas K133A reduced both ifnar2 binding affinity and biological activity to a similar degree. The antiviral and anti-proliferative activity of the multiple IFNβ mutant V147A/R151A/Y154A/N157A (all located on the E-helix) is less than 10-fold smaller compared with wild-type activity. Conversely, summing up the contributions of individual mutations on homologous positions on IFNα2 (Ala-145, Arg-149, and Ser-152) implies a reduction of about 300-fold in activity, suggesting that the E-helix might be more important for IFNα2 activity than for IFNβ. Thus it appears that, although IFNα2 and IFNβ bind ifnar2 on the same structural motifs, the distribution of binding energies within the binding site is different. Analogously, it has been shown that the relative importance of residues on ifnar2 toward IFNα2 and IFNβ differs significantly (17, 32).

IFNα2 and IFNγ share no obvious sequence or overall structural homology. However, helix A, the AB-loop, and the F-helix of IFNγ (which constitute the receptor I binding site) overlay onto helix A, the AB-loop, and the E-helix of IFNα2 with a root mean squared deviation of 2.3 Å for 59 residues (see Fig. 8 and Ref. 8). Interestingly, residues that participate in the IFNγ and IFNα2 receptor interactions are located at the same positions on the two helices and on the AB-loop (Fig. 8). This may suggest that ifnγR binds IFNγ in a similar orientation as ifnar2 binds IFNα2. Despite the good structural homology between the binding sites of these two IFNs, there is little sequence homology between the active site residues of these two proteins. Helix D of IFNα2 does not overlay any IFNγ helix using this structural alignment.

The biological activity of interferon is exerted through binding ifnar1 and ifnar2, the association of which causes the activation of multiple signal transduction pathways. Having available a large set of IFNα2 mutants with distinct affinities and rate constants of binding ifnar2, we were able to elucidate the role of IFN binding to ifnar2 for anti-viral and anti-proliferative activity in quantitative terms. Thus, the first event activating the signal transduction cascade was correlated with markers for the final steps of two important, different signal transduction pathways induced by IFNs. The linear correlation of both anti-viral and anti-proliferative activities with the relative binding affinity observed for all mutants analyzed suggests that IFNα2 binding is a rate-limiting event in activating the biological response. This result clearly establishes that the binding affinity of IFNα2 to its receptor does not surpass the requirements for cellular activity, as found for human growth hormone (34) and proposed for IFNβ (33). Further quantitative mechanistic interpretation of the affinity-activity relationship requires a closer look at parameters determining anti-proliferative and anti-viral activities; the assay for anti-proliferative activity is based on a continuous inhibition of cell growth and therefore may be considerably distorted by experimental variables such as cell growth rates, incubation times, or sample volumes. Interpretation of this data in absolute quantitative terms is therefore not appropriate. In contrast, anti-viral activity is an unbiased parameter, because cells are either protected or lysed by the virus attack. Therefore, further interpretations are based on this data. On a double logarithmic scale,

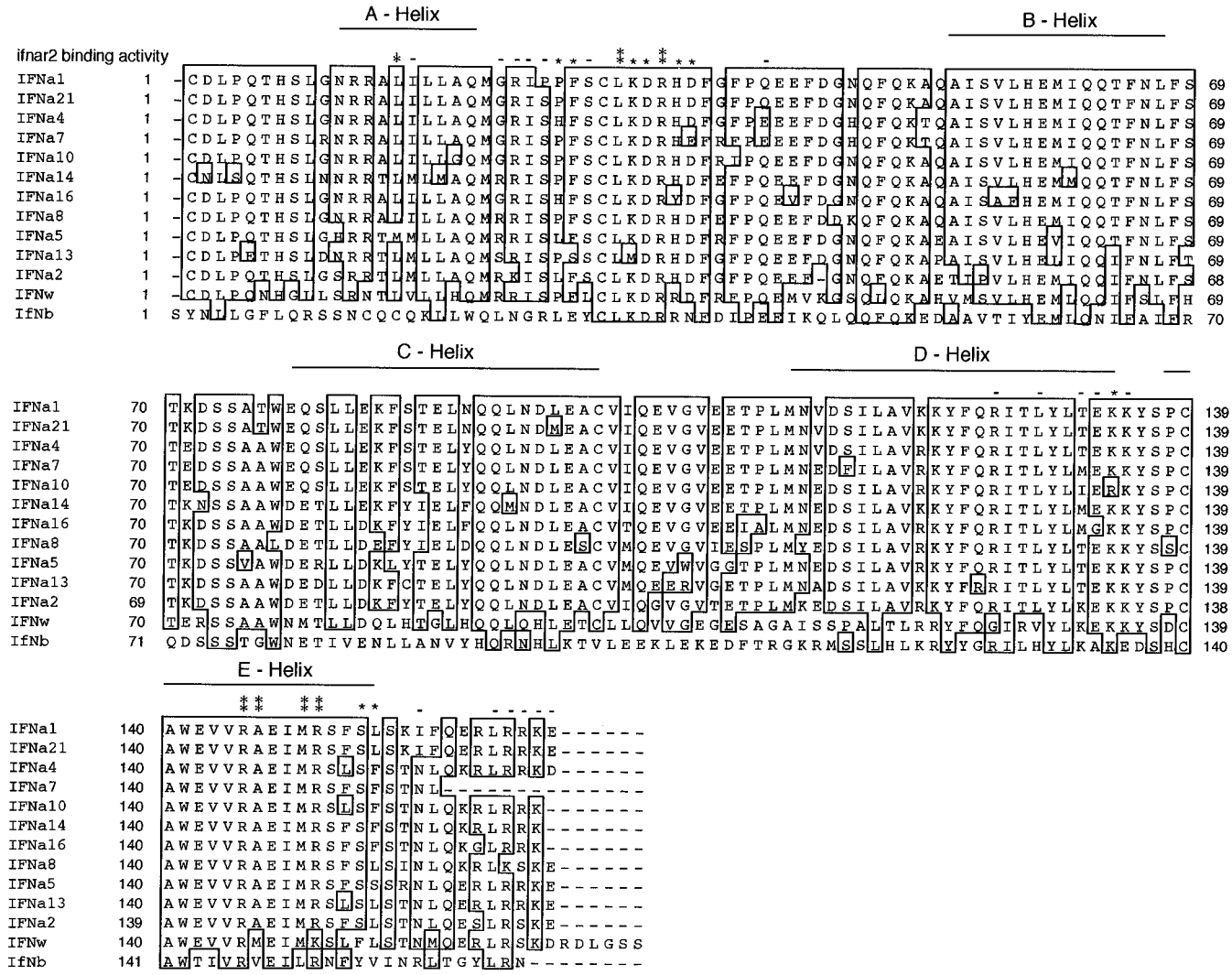

FIG. 7. **Sequence alignment of several type I IFNs.** In the *upper row*, the location of all residues of IFNα2 that were mutated are marked as follows: residues that do not contribute to binding (−), residues that contribute 0.5–2.0 kcal/mol (*one asterisk*), and residues that contribute more than 2 kcal/mol (*two asterisks*).

the linear correlation of IFN affinity with its anti-viral activity yielded a slope 0.72 ± 0.02. Because the logarithm of the affinity is a measure for the free energy ΔG^0 of binding, the relative anti-viral potency p_{AV} can be described by the function,

$$\log(p_{AV}) = \log(p_{AV,0}) + k\Delta G^0_{ifnar2} \qquad \text{(Eq. 1)}$$

where $G^0_{ifnar2}$is the free energy of the ifnar2·EC-IFNα2 complex for the different mutants. The correlation coefficient k in this equation is 1.34 mol/kcal, with $p_{AV,\,0}$ being $\sim 3 \times 10^{-7}$. What does this constant offset mean? Because IFN binds to both ifnar1 and ifnar2 on the cell surface, the binding affinity toward ifnar2 is enhanced by cooperative binding of ifnar1. Thus, typically a 10–100-fold higher affinity constant is observed for IFN binding to the cell surface receptor than for ifnar2 alone (35). The constant offset in Equation 1 most likely accounts for this constant energetic contribution of ifnar1 to form the ternary complex, and the value p_{AV} is in good agreement with the relative contribution of ifnar1. This result impressively corroborates that anti-viral activity is directly related to the number of occupied cell surface receptors. We therefore looked into the dose-time relationships of the activation of the cellular response. Picomolar concentrations of IFN are sufficient to achieve sufficient activation for anti-viral protection. At a concentration of 4 pM wild-type IFNα2 (~50% inhibition in the

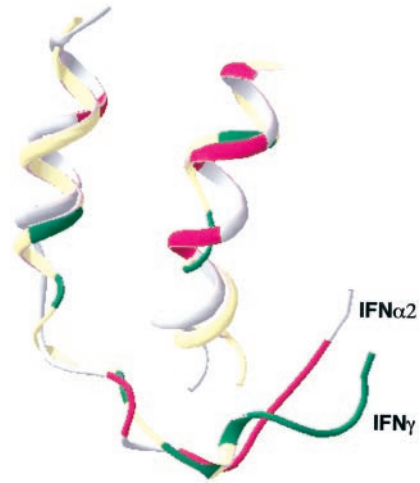

FIG. 8. **Structural alignment of the A-helix, the AB-loop, and the F-helix of IFNγ (the receptor I binding site) onto the A-helix, the AB-loop, and the E-helix of IFNα2.** The root mean squared deviation for the 40 overlaid residues is 2.9 Å. IFNγ is colored *yellow* and *green* (*green* for residues interacting with receptor 1 as determined from the structure (37)), IFNα2 is colored *gray* and *red* (*red* for residues interacting with ifnar2 as determined in this work).

anti-viral assay), ~8 receptors per cell will be occupied by IFN, assuming a K_D of 400 pM for the ternary complex and a total of 500 receptors per cell typical for WISH-cells. Thus, the concentration required for inducing anti-viral activity corresponds to only very few occupied receptors per cell, and higher doses should linearly increase the number of activated receptors. However, occlusion of IFNα2 after different incubation periods indicated that activation is necessary over at least 4 h and cannot be compensated by higher doses over longer time periods. This result is in good agreement with the observation that the half-life of phosphorylated STAT1 and STAT2 is short, and therefore continuous tyrosine kinase activity of Jak1 and Tyk2 is required for prolonged transcription (25).

The quantitative high-resolution description of the functional epitope of IFNα2 for binding, and the strict correlation of binding affinity with both anti-viral and anti-proliferative activity, are important steps forwards in understanding IFN recognition by its receptor on a molecular level. We showed that the E-helix constitutes the center of the ifnar2 binding site, in excellent analogy to several other homologous cytokines. Binding affinity seems to be driven by hydrophobic forces, whereas association is driven by electrostatic complementarity. Structural differences between complexes of ifnar2 with different IFNs are probably minor, only the distribution of binding energy on essentially the same set of residues is different. How this translates into differences in activity has to be studied by structural tools. Based on the linear relation between affinity and activity we were able to explain dose and time dependency within the signal transduction pathway.

Acknowledgments—We thank Hans-Martin Haake from the group of Günter Gauglitz, University of Tübingen, for supporting the setup and maintenance of the RIfS system. The anti-ifnar2-EC mAbs 46.10 and 117.7 were a generous gift from Daniela Novick at the Weizmann Institute of Science. Anti-viral activity assays were carried with valuable help from Sarah Barak of the Weizmann Institute of Science.

REFERENCES

1. Uzé, G., Lutfalla, G., and Gresser, I. (1990) *Cell* **60,** 225–234
2. Novick, D., Cohen, B., and Rubinstein, M. (1994) *Cell* **77,** 391–400
3. Der, S. D., Zhou, A., Williams, B. R., and Silverman, R. H. (1998) *Proc. Natl. Acad. Sci. U. S. A.* **95,** 15623–15628
4. Platanias, L. C., and Fish, E. N. (1999) *Exp. Hematol.* **27,** 1583–1592
5. Rani, M. R. S., Foster, G. R., Leung, S., Leaman, D., and Stark, G. R. (1996) *J. Biol. Chem.* **271,** 22878–22884
6. Sprang, S. R., and Bazan, J. F. (1993) *Curr. Opin. Struct. Biol.* **3,** 815–827
7. Senda, T., Matsuda, S., Kurihara, H., Nakamura, K. T., Kavano, G., Shimizu, H., Mizuno, H., and Mitsui, U. (1992) *EMBO J.* **11,** 3193
8. Radhakrishnan, R., Walter, L. J., Hruza, A., Reichert, P., Trotta, P. P., Nagabhushan, T. L., and Walter, M. R. (1996) *Structure* **4,** 1453–1463
9. Klaus, W., Gsell, B., Labhardt, A. M., Wipf, B., and Senn, H. (1997) *J. Mol. Biol.* **274,** 661–675
10. Karpusas, M., Nolte, M., Benton, C. B., Meier, W., Lipscomb, W. N., and Goelz, S. (1997) *Proc. Natl. Acad. Sci. U. S. A.* **94,** 11813–11818
11. Radhakrishnan, R., Walter, L., Subramaniam, P. S., Johnson, H. M., and Walter, M. R. (1999) *J. Mol. Biol.* **286,** 151–162
12. Mitsui, Y., Senda, T., Shimazu, T., Matsuda, S., and Utsumi, J. (1993) *Pharmacol. Ther.* **58,** 93–132
13. Seto, M. H., Harkins, R. N., Adler, M., Whitlow, M., Church, W., and Croze, E. (1995) *Protein Sci.* **4,** 655–670
14. Uzè, G., Lutfalla, G., and Mogensen, K. E. (1995) *J. Interferon Res.* **15,** 3–26
15. Mogensen, K. E., Lewerenz, M., Reboul, J., Lutfalla, G., and Uze, G. (1999) *J. Interferon Cytokine Res.* **19,** 1069–1098
16. Piehler, J., and Schreiber, G. (1999) *J. Mol. Biol.* **289,** 57–67
17. Piehler, J., and Schreiber, G. (1999) *J. Mol. Biol.* **294,** 223–237
18. Albeck, S., and Schreiber, G. (1999) *Biochemistry* **38,** 11–21
19. Brecht, A., Gauglitz, G., and Polster, J. (1993) *Biosens. Bioelectron.* **8,** 387–392
20. Gauglitz, G., Brecht, A., Kraus, G., and Nahm, W. (1993) *Sensor Actuat. Biol. Chem.* **11,** 21–27
21. Schmitt, H. M., Brecht, A., Piehler, J., and Gauglitz, G. (1997) *Biosens. Bioelectron.* **12,** 809–816
22. Rubinstein, S., Familletti, P. C., and Pestka, S. (1981) *J. Virol.* **37,** 755–758
23. Chang, N. T., Kung, H. F., and Pestka, S. (1983) *Arch. Biochem. Biophys.* **221,** 585–589
24. Cheetham, B. F., McInnes, B., Mantamadiotis, T., Murray, P. J., Alin, P., Bourke, P., Linnane, A. W., and Tymms, M. J. (1991) *Antiviral Res.* **15,** 27–39
25. Lee, C. K., Bluyssen, H. A. R., and Levy, D. E. (1997) *J. Biol. Chem.* **272,** 21872–21877
26. Korn, A. P., Rose, D. R., and Fish, E. N. (1994) *J. Interferon Res.* **14,** 1–9
27. Clackson, T., and Wells, J. A. (1995) *Science* **267,** 383–386
28. Bogan, A. A., and Thorn, K. S. (1998) *J. Mol. Biol.* **280,** 1–9
29. Lijnzaad, P., Berendsen, H. J. C., and Argos, P. (1996) *Proteins* **26,** 192–203
30. Selzer, T., and Schreiber, G. (1999) *J. Mol. Biol.* **287,** 409–419
31. Selzer, T., Albeck, S., and Schreiber, G. (2000) *Nat. Struct. Biol.* **7,** 537–541
32. Lewerenz, M., Mogensen, K. E., and Uze, G. (1998) *J. Mol. Biol.* **282,** 585–599
33. Runkel, L., deDios, C., Karpusas, M., Betzenhauser, M., Muldowney, C., Zafari, M., Benjamin, C. D., Miller, S., Hochman, P. S., and Whitty, A. (2000) *Biochemistry* **39,** 2538–2551
34. Pearce, K. J., Cunningham, B. C., Fuh, G., Teeri, T., and Wells, J. A. (1999) *Biochemistry* **38,** 81–89
35. Cohen, B., Novick, D., Barak, S., and Rubinstein, M. (1995) *Mol. Cell. Biol.* **15,** 4208–4214
36. Guex, N., and Peitsch, M. C. (1997) *Electrophoresis* **18,** 2714–2723
37. Walter, M. R., Windsor, W. T., Nagabhushan, T. L., Lundell, D. J., Lunn, C. A., Zauodny, P. J., and Narula, S. K. (1995) *Nature* **376,** 230–235